Experimental Eye Research 145 (2016) 100–109

Contents lists available at ScienceDirect

Experimental Eye Research

journal homepage: www.elsevier.com/locate/yexer

Research article

Protein profiles in cortical and nuclear regions of aged human donor lenses: A confocal Raman microspectroscopic and imaging study

Gijs F.J.M. Vrensen [a], Cees Otto [b], Aufried Lenferink [b], Barbara Liszka [b], Gustavo A. Montenegro [c], Rafael I. Barraquer [c], Ralph Michael [c, d, *]

[a] Department of Ophthalmology, Leiden University Medical Center, University of Leiden, The Netherlands
[b] Medical Cell Bio Physics, University of Twente, Enschede, The Netherlands
[c] Institut Universitari Barraquer, Universitat Autònoma de Barcelona, Barcelona, Spain
[d] University Eye Clinic, Paracelsus Medical University, Salzburg, Austria

ARTICLE INFO

Article history:
Received 17 June 2015
Received in revised form
26 October 2015
Accepted in revised form 10 November 2015
Available online 22 November 2015

Keywords:
Lens aging
Nuclear cataract
Cortical cataract
Raman spectroscopy
Raman imaging
Hierarchical cluster analysis

ABSTRACT

A combination of Raman spectroscopy, imaging, hierarchical cluster analysis (HCA) and peak ratio analysis was used to analyze protein profiles in the superficial cortex (SC), deep cortex (DC) and nucleus of old human lenses with cortical, nuclear and mixed cataracts.

No consistent differences were observed in protein spectra and after cluster analysis between the three locations irrespective of the presence or absence of cortical opacities and/or coloration. A sharp increase (~15%–~33%) in protein content from SC to DC, normal for human lenses, was found in 7 lenses. In 4 lenses, characterized by the absence of cortical opacities, the SC has a protein content of ~35%. A significant increase in the disulfide-to-protein ratio is found only in the SC of the 7 cortical cataracts. No changes were found in sulfhydryl-to-protein ratio. The relative contents of α-helices and β-sheets increase from SC to nucleus. β-Sheets are more common in the SC of lenses with cortical cataract.

The absence of significant and consistent changes in protein profiles between nucleus and cortex even in cases of severe coloration is not favoring the prevailing concept that ubiquitous protein oxidation is a key factor for age related nuclear (ARN) cataracts. The observations favor the idea that multilamellar bodies or protein aggregates at very low volume densities are responsible for the rise in Mie light scatter as a main cause of ARN cataracts leaving the short-range-order of the fiber cytoplasm largely intact. The absence of significant changes in the protein spectra of the deep cortical opacities, milky white as a result of the presence of vesicle-like features, indicate they are packed with relatively undisturbed crystallins.

1. Introduction

The purpose of the eye lens is to project a sharply focused, undistorted image of the visual surround on the neural retina. Requirements securing this purpose are transparency, a high refractive index, accommodative power and low scattering properties which are realized by specific structural and functional properties of the lens.

The inherent transparency of the eye lens is due to the absence of blood cells and blood vessels and the large organelle free zone encompassing the deep cortex and core attributable to the pre-programmed elimination of nuclei and cell organelles of elongating lens fibers (Bassnett, 2009; Dahm et al., 2011; Vrensen et al., 2004).

The human eye lens is characterized by a sharp gradient in refractive index (RI) and protein content. Within about 0.5 mm from the capsular surface RI is rising from ~1.37 in the epithelium and elongating fibers plateauing to a constant level of ~1.42 in the cortical and nuclear regions (Augusteyn, 2008). Accommodation amplitude (AA) decreases with age from 19 to 2 D due to changes in the nuclear stiffness and decline in the functioning of the ciliary body (Dubbelman et al., 2003). This decline in AA is a main factor for presbyopia.

The low scattering properties of lens fibers are due to the short-range-order of the crystallins (Delaye and Tardieu, 1983), the absence of refractive index differences between cytoplasm and membranes of the fibers (Michael et al., 2003) and the refractive

* Corresponding author. Institut Universitari Barraquer, Laforja 88, E-08021, Barcelona, Spain.
E-mail address: ralphm@barraquer.com (R. Michael).

http://dx.doi.org/10.1016/j.exer.2015.11.009
0014-4835/

index matching between the cytoplasm of adjacent cells achieved through the formation of cellular fusions that allows the intermingling of proteins (Bassnett et al., 2011).

The eye lens grows throughout life. Post-mitotic epithelial cells in the equatorial zone continuously form new fibers all be it at a low rate. Cohorts of fibers are stacked one upon another in rows and are held together by complex interdigitating protrusions (Bassnett et al., 2011; Dickson and Crock, 1972; Kuszak et al., 2004; Vrensen and Willekens, 1990). The lens is a closed system and, in contrast with most other tissues, there is no shedding of fibers during its lifetime. Furthermore in the absence of metabolic activity in the organelle free zone there is no turnover of the crystallins. Hence lens fiber proteins are as old as their time of origin i.e. central fibers are as old as the individual. They are therefore subject to aging factors for long periods which eventually lead to cortical and nuclear cataracts (Lou, 2003; Michael and Bron, 2011; Vrensen, 2009). It is advocated that these changes are accompanied or induced by conformational changes and aggregation of crystallins and disturbance of the short range order (Truscott, 2005).

Although many factors have been proposed to contribute to age related cataract in humans, recent data indicate that aging as such is by far the most prominent causative factor (Michael and Bron, 2011; Truscott, 2000, 2005). Based on slitlamp, Scheimpflug and retro-illumination images three primary types of age-related cataracts can be distinguished; nuclear (NC), cortical (CC) and posterior sub-capsular (PSC) cataracts. In addition many lenses show mixed types of cataract. The sample of donor lenses used in this study, indeed represent a broad spectrum of age related nuclear and cortical cataracts (Fig. 1). PSC's are far less common in the population (<1%) (Sasaki et al., 2004) and are absent in the sample.

Nuclear cataracts are clinically characterized by an age-related increase in straylight, coloration and fluorescence of the lens core, starting to have significant vision effects around the age of 40–50 years (Burd et al., 2012; Truscott, 2000, 2005; van den Berg, 1996; van den Berg and IJspeert, 1995). Coloration and fluorescence of the lens nucleus are caused by accumulation of chromophores induced by UV-irradiation and oxidative stress (Davies and Truscott, 2001). Oxidative stress also leads to changes in crystallins as racemization, deamidation and truncation of crystallins, loss of sulfhydryl groups of cysteine and methionine and to aggregation of proteins. A decline in the availability of glutathione (GSH) around the age of 40–50 years is proposed as being a main cause of this effect of oxidation in old age (Michael and Bron, 2011; Truscott, 2005).

In a recent paper Michael et al. (2014) showed that Raman microspectroscopy is a powerful analytical tool to approach local changes in protein and lipid profiles with a resolving power at the sub-μm level. In the present study we used this technique to analyze the protein profiles of superficial cortical, deep cortical and nuclear regions of old human autopsy lenses with nuclear, cortical and mixed cataracts.

2. Material and methods

Lenses from 11 donors (Fig. 1) were provided by the Banco de Ojos para Tratamientos de la Ceguera, Barcelona in collaboration with the Neurological Tissue Bank of the Biobank-Hospital Clinic-IDIBAPS (NTB-IDIBAPS), Barcelona. Written informed consent for removal of the eyes for diagnostic and research purposes was obtained from the patients and/or their relatives. The research adhered to the tenets of the Declaration of Helsinki on research involving human subjects.

Cortical cataracts were graded for percentage of lens circumference affected by cortical opacities and their extension from the lens periphery towards the optical axis. Nuclear cataracts were graded in a combined scale for opacity and coloration on a scale between 0 and 10. Grading was performed by three independent ophthalmologists, and the mean grading values are given in Table 1. Lens tissue was fixed in 3.6% PBS buffered formaldehyde for 4 weeks. Half lenses were cut with parallel placed razorblades in slices of about 0.5 mm thickness and stored in PBS for Raman analysis. The cortex of the lenses was analyzed at about 0.15 mm (superficial cortex) and 0.7 mm (deep cortex) below the equatorial lens capsule. Cortical opacities are usually located at 0.7 mm. The nucleus was analyzed at about 4 mm below the equatorial lens capsule (Fig. 2).

Non-resonant Raman spectroscopy and imaging experiments were performed on a previously described laser-scanning confocal Raman microspectrometer (Pully et al., 2010). The system consist of a Krypton laser (Innova 90-K; Coherent, SantaClara, CA, λ_{exc} 647.1 nm), an upright microscope BX41 from Olympus with an objective Olympus, Plan Apochomat, 40×, 0.95NA, coverslip corrected for illumination of the sample as well as for collection of Raman scattered photons. The home-built spectrograph was optimized for broadband (20–3670 cm^{-1}) high-wave number-resolution (1.85–2.85 cm^{-1}/pixel) Raman microspectroscopy. Imaging experiments were performed by raster-scanning the laser beam over a region of interest with a step size of approx. 0.5 μm (30 × 30 μm^2 containing 64 × 64 spectra) with a dwell time per pixel of 50 ms. A full image of each area was thus acquired in ~205 s with a laser power of 35 mW. Noise in the resulting 3D (spatial × spatial × spectral dimension) data matrix of 4096 spectra times 1600 frequencies was reduced by singular value decomposition (Uzunbajakava et al., 2003). In the three areas (Fig. 2) of each lens three Raman datasets per area were acquired to a total of 99 Raman datasets, each containing 4096 Raman spectra. All together the analysis concerned 405,504 Raman spectra.

The main objective of this study is the analysis of the difference in protein profiles of the three lens regions indicated. Because the lens mainly consists of lens fibers with a high protein content and have no cell organelles, except for a small equatorial region, integrated spectra over the 30 × 30 μm^2 areas can be considered to reflect the protein profile of the region measured. Three measurements per region are averaged and the background, mainly due to fluorescence, is removed by subtracting a linear function (Fig. 2). For the so-called fingerprint region (700–1800 cm^{-1}), this function was obtained by a linear fit through the intensity at 800 cm^{-1} and at 1830 cm^{-1}. For comparison of the profiles of the three areas, the spectra are normalized for protein using the 1450 cm^{-1} protein band as described by Siebinga et al. (1992) (Fig. 2). For the high frequency region (2700–3700 cm^{-1}), this function was obtained by a linear fit through the intensity at 2440 cm^{-1} and at 2770 cm^{-1} (Fig. 2).

Protein mass percentage (PMP) was calculated according to Huizinga et al. (1989) from the background corrected ratios of the Raman peaks at 3390 cm^{-1} (water peak) and 2935 cm^{-1} (CH-stretch of proteins). For the relative contributions of β-sheets (1668 cm^{-1}), α-helices (1265 cm^{-1}), phenylalanine (1000 cm^{-1}), tyrosine (857 cm^{-1}), disulfide (S–S)(508 cm^{-1}) and sulfhydryl (SH)(2581 cm^{-1}) the ratios of the corresponding Raman signals and the protein Raman signal at 1450 cm^{-1} were calculated for all the lenses and sites. Mean values of the ratios were calculated as well as the coefficient of error. We also calculated the coefficient of error for the full spectra of the 11 lenses. Differences were tested using Student's t-test.

Another point of interest is the problem of the occurrence of specific objects within the measured areas as for instance protein aggregates. To this end hierarchical cluster analysis (HCA) was performed on Raman imaging data matrices to visualize regions with high Raman spectral similarities. No baseline subtraction was performed prior to principal component analysis (PCA). In the cluster analysis routine scores derived from PCA were taken as input variables, squared Euclidean distances were used as distance

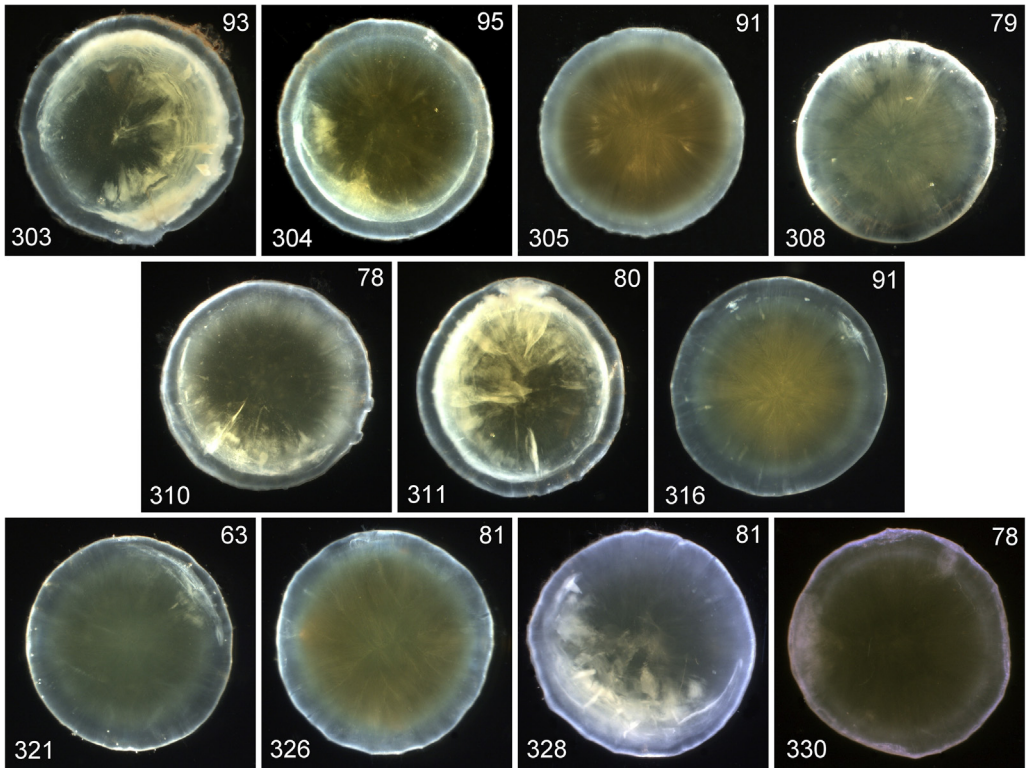

Fig. 1. Panel of darkfield images of the human donor lenses studied in this paper. Note the diversity of nuclear coloration and extension of milky white cortical opacities. For details see Table 1.

measure, and Ward's algorithm was employed to partition Raman datasets into clusters (van Manen et al., 2005). In the present study we have chosen the 8 cluster analysis since it most clearly visualizes local differences. The cluster analysis is performed for the fingerprint region (1100–1750 cm^{-1}). The Raman spectra in the Raman imaging data matrices are not corrected for background and not normalized for protein content prior to PCA and HCA to provide an unbiased analysis. The white light and false color coded images of the fingerprint region are shown annex to the spectra.

mature cortical cataracts (303, 311, 328), to opacities restricted to small peripheral regions (304, 310, 316, 321) and lenses with no signs of peripheral opacities (305, 308, 326, 330). All lenses show nuclear coloration. Based on ophthalmological screening nuclear changes range from nearly zero (303, 311) to dense (305) (Table 1).

Fiber dissociations and aggregation of lens proteins are proposed to play a key role in the formation of cortical and nuclear cataracts. Therefore we may expect significant changes in the Raman profiles between lenses with and those without cortical and nuclear cata-

Table 1
Donor information and lens cortical and nuclear findings.

Donor	Age (years)	Sex	Circumference affected[a]	Extension to optical axis[b]	Nuclear cataract[c]
305b	91	m	0	0	6
308a	79	f	0	0	1
326a	81	m	0	0	4
330a	78	f	0	0	2
316a	91	f	XX	XX	4
321a	63	f	XX	XX	2
304a	95	f	XXX	XXX	4
310b	78	f	XXX	XXXX	1
328b	81	m	XXXX	XXXXX	1
303a	93	f	XXXXX	XXXXX	1
311a	80	f	XXXXX	XXXXX	1

Donors collected between May and December 2011; m: male; f: female.
[a] Degree of lens circumference affected by cortical opacity: 0% = 0; 1…20% = x; 21…40% = xx; 41…60% = xxx; 61…80% = xxxx; 81…100% = xxxxx (100% means entire lens circumference affected.).
[b] Extension of the cortical opacity towards the optical axis is expressed as smallest diameter of a theoretical pupil where the cortical opacity would be visible inside the pupillary area: no cortical opacity = 0; 8.1…10 mm = x; 6.1…8.0 mm = xx; 4.1…6.0 mm = xxx; 2.1…4.0 mm = xxxx; 0. 2 mm = xxxxx.
[c] Nuclear cataracts graded in a combined scale for opacity and coloration scales from 0 to 10.

3. Results

Darkfield images (Fig. 1) and ophthalmological screening (Table 1) indicate that the 11 lenses studied represent a broad spectrum of lens changes. Cortical changes range from rather

racts provided the Raman samples indeed represent altered/affected parts of the lenses. To validate this, white light images were taken of all Raman areas analyzed. As exemplified in Fig. 3 A, B and D white light images allow discrimination of areas with and without opacities. The superficial and nuclear sites all showed regularly

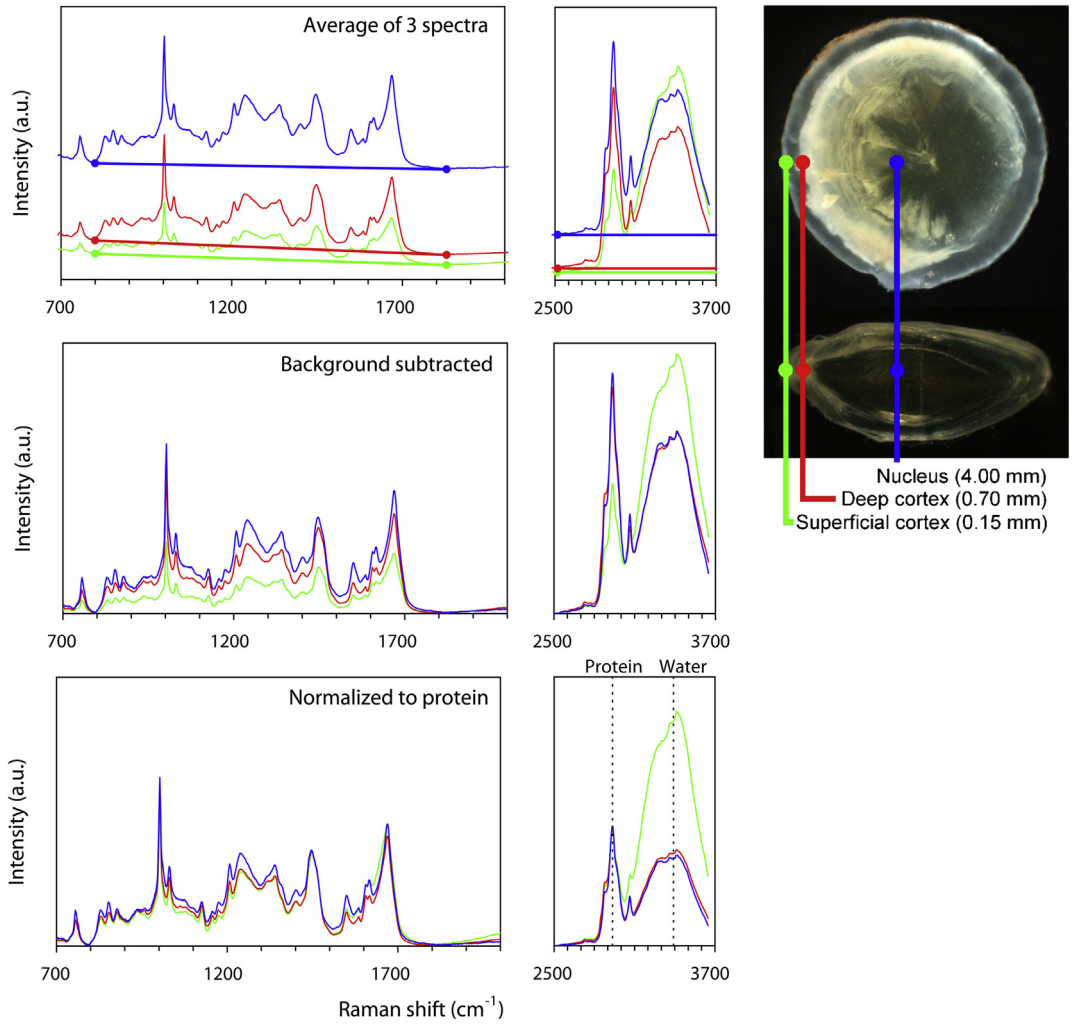

Fig. 2. Explanatory panel illustrating the location of the superficial cortical (0.15 mm, green), deep cortical (0.70 mm, red) and nuclear (4.0 mm, blue) sites at which the low and high frequency Raman spectra were collected in 30 × 30 μm^2 samples. Each individual sample was screened 3 times. The 3 spectra are averaged and subsequently the background was subtracted. For comparison these spectra were normalized for protein content using the protein peak at 1450 cm^{-1}. Note the high water peak at 3390 cm^{-1} in the superficial cortex. Raman peaks indicated by a dotted line: 2935 cm^{-1} CH-stretch of proteins and 3390 cm^{-1} water.

organized fibers only (Fig. 3 A). In 5 out of the 11 lens samples deep cortical sites exhibited opacities as illustrated in Fig. 3 B and D. They closely resemble opacities as previously described by electron microscopy (Fig. 3 C and E–G). In 4 of the samples there are no globular/vesicular opaque elements and 2 are questionable.

In Fig. 4 the Raman spectra, corrected for fluorescence and normalized for protein content, of all the lenses analyzed are plotted for SC (0.15 mm), DC (0.7 mm) and nucleus (4.0 mm). We have calculated the Coefficient of Error (CE) of the Raman signal for the 11 lenses in Fig. 4. CE was below 5% except for wavenumbers with very low Raman intensities (corresponding to wavenumbers with no Raman peaks) and except for the region around 1500 cm^{-1}, where it was around 10%. Because of this small variation, we have calculated the mean of all 11 lenses and presented this in Fig. 5.

A topic of interest for the etiology of cataract is whether aging per se is leading to protein changes. Given the absence of significant differences in the Raman spectra, among lenses with and without nuclear and/or cortical cataracts, it seems justified to compare the mean values of the three regions (Fig. 5). They represent age differences between several weeks post-conception (deep nucleus) and the more recently formed fibers (superficial cortex) spanning a period of 63–95 years in our lens sample. As shown in Fig. 5 the difference in life span of lens fibers does not lead to major changes in the Raman spectra. In the lens nucleus there are somewhat higher Raman intensities in the Amide III region and the signals for the aromatic amino acids phenylalanine, tyrosine and tryptophan (see also Table 2).

Hierarchical cluster analysis visualize areas with high Raman spectral similarities and thus may reflect specific objects in the 30 × 30 μm^2 samples. For HCA the basic spectra are not corrected for fluorescence and not for protein content. Fig. 6 shows a sample with regularly organized lens fibers with no dissociations. Although the false color image suggest local differences, the spectra only represent minimal changes in intensity due to small differences in local protein content and/or fluorescence. Fig. 7 illustrates one out of the 5 deep cortical lens samples showing an area with and without globular dissociations of lens fibers. No marked qualitative changes in the Raman spectra are observed except for fluorescent background. We also analyzed a region with marked differences in the HC image (Fig. 8). The white/blue regions have Raman spectra almost identical to those found in Figs. 6 and 7 and reflect the dominating protein signals of the fiber cytoplasm. The small red and orange regions in the image have deviating spectra. Peak assignments according to Bergner et al. (2012) reveal the presence of Raman signals reflecting relative high concentrations of lipids and cholesterol. The Raman imaging datasets of the lenses presented in Figs. 6–8 were also analyzed simultaneously with PCA to reveal

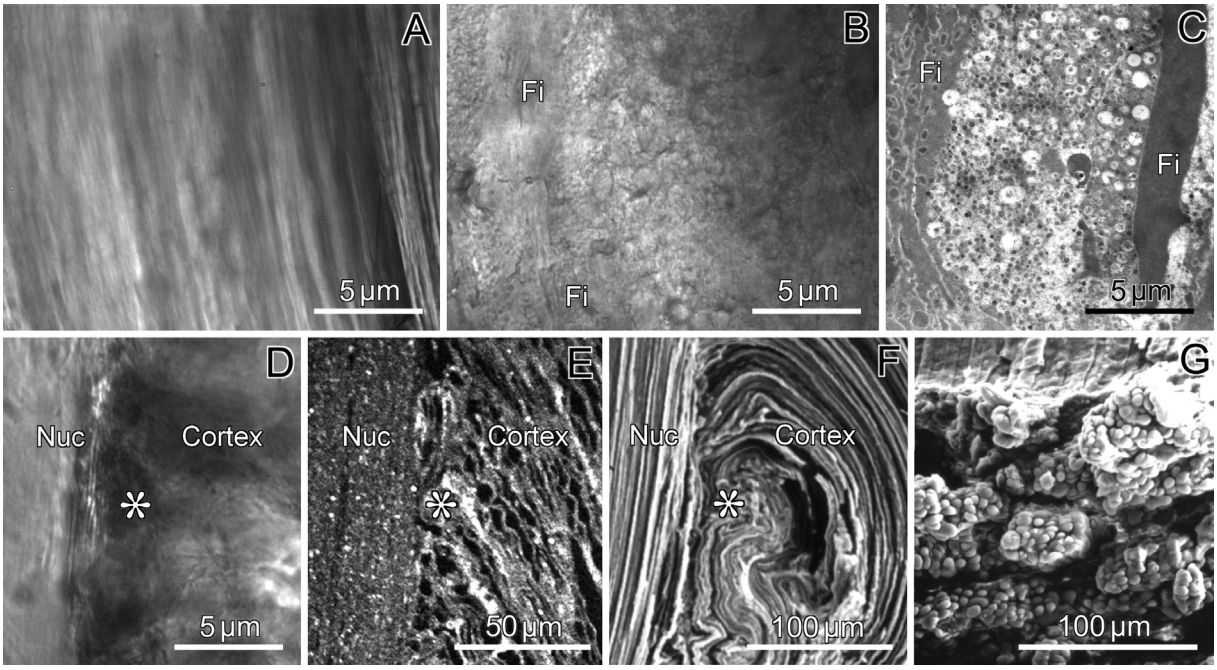

Fig. 3. Panel showing representative white light images (LM) (A, B and D) of deep cortical sites of the lens slices analyzed in the present study. In A only regularly organized fibers are seen. They are common in lenses with nuclear cataract only and in some samples with minor cortical opacities. B illustrates a deep cortical region in a lens with an opacity showing a globular aspect. In previous studies identical regions have been described as dot and shade-like opacities and TEM observations show accumulation of globular/vesicular elements (C). Undistorted fibers (Fi) are found annex to the globular elements. In D, E and F (*) rather complex forms of opacities (cuneiform cataract) are illustrated characterized by distorted and broken fibers at the nuclear cortical interface in both white light images as used in the present study (D) and in fluorescence images after DiC18 staining for membranes (E). The low power SEM image (F) shows an identical distorted morphology of lens fibers at this interface which when viewed at a different angle and higher magnification exhibit accumulation of globular elements (G). For details of the TEM, SEM and fluorescence images see Brown et al. (1993); Michael et al. (2008); Vrensen and Willekens (1990) (TEM: transmission electron microscopy, SEM: scanning electron microscopy. The TEM image of C is a courtesy of Dr. Paul Jap, Radboud University Nijmegen, NL).

directly correspondences or differences. For this purpose the datasets of the three regions in the SC were combined with those of the three regions in the DC and the N. In this way a dataset was formed consisting of 9 times 4096 Raman spectra. The first principal component (PC) for lens 316, lens 311 and lens 310 were respectively 97.2%, 97.4% and 96.7% while the second PC carried respectively ~1%, ~0.5% and ~1.2% of the variance in the total dataset. Therefore it can be concluded that the Raman spectra of the superficial cortex, the deep cortex and the nucleus are very similar to each other.

We calculated the protein mass percentage (PMP) according to the protocol of Huizinga et al. (1989) using the protein and water peaks at 2935 cm^{-1} and 3390 cm^{-1} respectively (see Fig. 2). A remarkable aspect of the present observations is that out of the 11 lenses 4 lenses have a high PMP at the 0.15 mm site in contrast with a low PMP in the other 7 lenses. DC (0.70 mm) and nuclear (4.0 mm) sites of all lenses have about equal PMP's (Fig. 9). We also calculated the protein ratios of the aromatic acids phenylalanine (1003/1453 cm^{-1}) and tyrosine (457/1453 cm^{-1}). These parameters also showed significantly higher values in the superficial cortex of lenses with no-cortical cataract (Table 2 (tyrosine not shown)). Because the aromatic signals used are mainly due to ring vibrations and hardly contribute to the protein signal at 1453 cm^{-1} they confirm the high protein content in the superficial cortex of no-cortical cataracts. Moreover, in cortical cataracts the phenylalanine and tyrosine signals increase with depth below the capsule which they do not do in the lenses with no cortical cataract.

We also analyzed changes in the relative disulfide content in the cortical cataract and non-cortical cataract lenses at three sample sites. Both the 508/622 cm^{-1} (Yu et al., 1985) and the 545/1453 cm^{-1} (not shown) ratios show a significantly higher ($p < 0.02$) disulfide content in the SC (0.15 mm) site in the cortical cataract lenses vs the noncortical cataract lenses (Table 2). The DC and nuclear sites in the cortical cataract lenses have significantly lower disulfide contents than the SC site. The sulfhydryl content analyzed using the 2581/2731 cm^{-1} ratio (Kuck et al., 1982) showed no significant changes among the two lens pathologies and the depth below the capsular surface (Table 2).

As shown lens crystallins in opacities have higher relative β-sheet contents than most other biological proteins (Michael et al., 2014) suggesting a possible relation between β-sheet content and opacification. Therefore we calculated the relative β-sheet content (1668/1450 cm^{-1}) for all lenses at all three sites (Table 2). We also calculated the relative α-helix content (1265/1450 cm^{-1}) for these lenses and sites (Table 2). The main observations are that for both α-helix and β-sheet the ratios increase with depth below the capsular surface except for the 0.15 mm site in the cortical cataracts which is significantly higher than in the non-cortical cataracts.

4. Discussion

The present Raman study shows that protein profiles in the nuclear region, i.e. the oldest part of the lens, do not significantly differ from protein profiles in the much younger DC and SC regions (Figs. 4 and 5). HCA reveals the absence of local variations in all samples of the 11 lenses analyzed. It can be opposed that the absence of marked changes is due to insufficiency to visualize small objects alongside the omnipresent protein spectrum that dominates the Raman spectrum. In the lens the overall phospholipid and cholesterol content is less than 5% of dry weight (Li et al., 1985; Siddique et al., 2010). The small red and orange regions in Fig. 8 however have deviating spectra with peaks for phospholipid and cholesterol (Bergner et al., 2012). The white light image shows that in this region lens fibers of opposing sides meet and may represent a suture line. Suture lines are characterized by complex interdigitating membranes from opposing fibers (Kuszak et al., 2004) and therefore will have high local (phospho)lipids and cholesterol

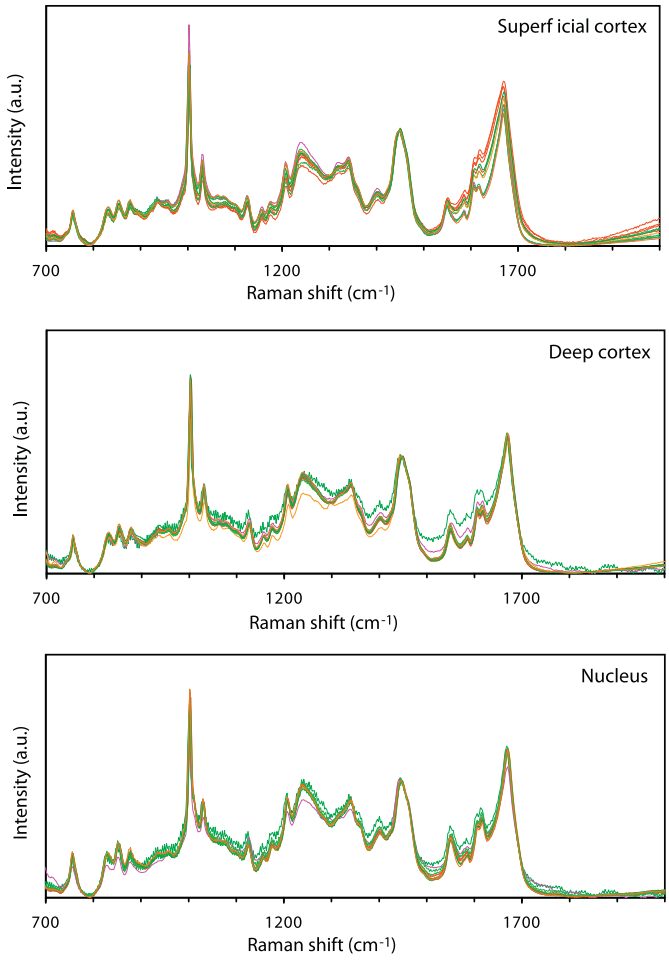

Fig. 4. In this figure the normalized spectra of all 11 lenses at the superficial, deep cortical and nuclear sites are plotted. As described under results the averages and coefficients of error were calculated for all three sites.

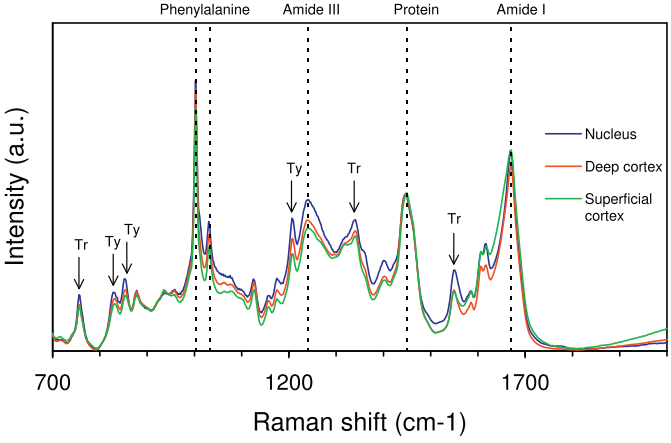

Fig. 5. This figure shows the averaged Raman spectra of all 11 lenses at the 3 locations as calculated from Fig. 4. Note that the 3 locations do not qualitatively deviate. Note further that the nuclear region has a somewhat higher Amide III band and that the phenylalanine, tyrosine (ty) and tryptophan (tr) peaks are a bit higher. Some main peaks are indicated.

contents. From this it can be concluded that the present Raman protocols have a resolution at the sub-μm level. This allows the conclusion that independent of the severity of the coloration, aging of lens crystallins does not lead to significant changes in protein

Table 2
Protein mass fractions and peak-to-protein ratios for α-helix, β-sheet, SH, S–S and tyrosine and phenylalanine of cortical (n = 7) and no cortical (n = 4) samples.

Location	**Protein mass fraction**				
	Cortical cataract		No cortical cataract		
	Mean	CE	Mean	CE	
0.15 mm	14.6*	6.7%	34.8	5.5%	**p < 0.001**
0.70 mm	32.6	6.2%	33.6	4.2%	p = 0.95
4.00 mm	32.7	1.9%	33.6	6.2%	p = 0.65
	Phenylalanine		1000/1450 cm^{-1}		
	Cortical cataract		No cortical cataract		
	Mean	CE	Mean	CE	
0.15 mm	1.47*	2.0%	1.69	0.9%	**p < 0.001**
0.70 mm	1.65	3.2%	1.66	2.8%	p = 0.77
4.00 mm	1.75	1.8%	1.72	3.6%	p = 0.86
	α-helix ratio		1265/1450 cm^{-1}		
	Cortical cataract		No cortical cataract		
	Mean	CE	Mean	CE	
0.15 mm	0.68	2.6%	0.73	0.4%	p = 0.08
0.70 mm	0.72	1.7%	0.77	2.4%	p = 0.08
4.00 mm	0.85*	1.4%	0.86**	3.7%	p = 0.70
	β-sheet ratio		1668/1450 cm^{-1}		
	Cortical cataract		No cortical cataract		
	Mean	CE	Mean	CE	
0.15 mm	1.33	0.8%	1.16	0.6%	**p < 0.006**
0.70 mm	1.17*	0.8%	1.19	0.8%	p = 0.029
4.00 mm	1.29	0.4%	1.26**	0.9%	p = 0.69
	S–S ratio		508/622 cm^{-1}		
	Cortical cataract		No cortical cataract		
	Mean	CE	Mean	CE	
0.15 mm	1.22*	8.3%	0.84	22.7%	**p = 0.014**
0.70 mm	0.93	15.6%	0.83	18.1%	p = 0.53
4.00 mm	0.87	14.3%	0.76	24.2%	p = 0.13
	SH ratio		581/2731 cm^{-1}		
	Cortical cataract		No cortical cataract		
	Mean	CE	Mean	CE	
0.15 mm	0.61	2.4%	0.59	7.6%	p = 0.54
0.70 mm	0.58	2.4%	0.63	8.7%	p = 0.08
4.00 mm	0.47	8.8%	0.61	7.4%	p = 0.25

All signals were corrected for background in the fingerprint and high frequency region.
Protein mass percentage calculated according to Huizinga et al. (1989).
SH = sulfhydryl ratio, calculated according to Yu et al. (1985). S–S = disulfide.
Significance at the 5% level between the 3 locations is indicated as * and between the lenses with and without cortical cataracts as **p-values** according to the outcome of Student's t-test.
Coefficient of error (CE) = SD/$\sqrt{n}$/mean × 100%.

profiles. This means that the present data are not in support of the view that ubiquitous unfolding, racemization, truncation and denaturation of crystallins (Truscott, 2000, 2005) are a dominating factor leading to aging. The present data are in line with the observations of Taylor et al. (1996) and Al-Ghoul et al. (1996) that the cytoplasm of nuclear fibers is extremely fine grained in normal lenses and in lenses with nuclear cataract and only incidentally show minor ultrastructural defects. This likely indicates that the short-range-order of the crystallins is only minimally disturbed and that the lenses are still largely transparent. According to Costello et al. (2010, 2012) a key observation in nuclear cataracts is a 7.5 fold increase in multi-lamellar bodies (MLB's) with a diameter of 1–4 μm and a refractive index of 1.47–1.53 i.e. significantly above that of the surrounding cytoplasm (1.42). The authors propose that Mie scattering of these MLB's is the main cause of increased

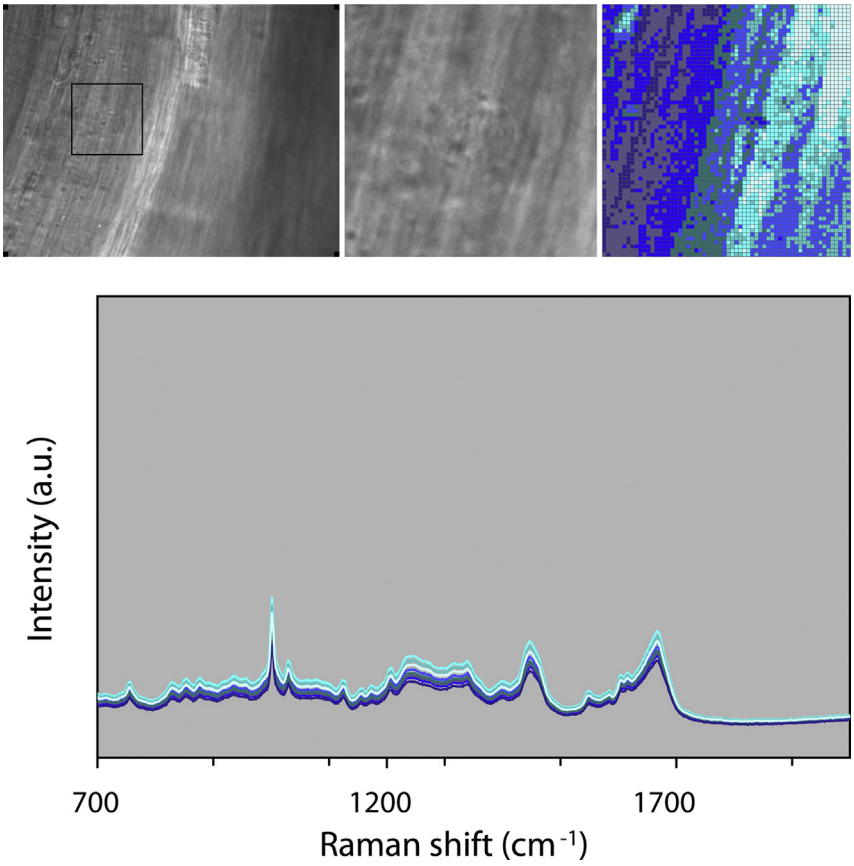

Fig. 6. Hierarchical cluster analyses of a 30 × 30 mm^2 sample of the superficial cortex of a lens with no aberrant fiber structures (upper left and upper middle images). The spectra of this sample are qualitatively all identical. The false color image (upper right) represents the distribution of these spectra over the sample. Although this suggests some local differences within the sample we have to realize these difference are extremely small and due to some minor local variations in background and water content (For details on HC analyses see material and methods.).

forward light scattering in age related nuclear cataracts. van den Berg (1996) proposed that aggregated proteins with a size of 0.7 μm or larger are an important cause of the increased forward light scatter. From our matrix data fractional areas can be calculated. The fractional areas of for instance the orange and red areas in Fig. 7 are 0.5 and 2% respectively and thus represent, in a matrix of 30 × 30 μm^2, approximately 4.5 and 9 μm^2. The protein aggregates of van den Berg (1996) have on average an area of at least 1.54 μm^2 and the MLB's of Costello et al. (2010, 2012) of 3.14–50.24 μm^2. Because of the spatial resolution of at least 4.5 μm^2 and the measured high refractive index of the MLB's, reflecting a considerable increase in local protein content (Costello et al., 2010), HC analysis would certainly have detected these structures. However, the volume density of the MLB's of Costello et al. (2010, 2012) and the spherical particles of van den Berg (1996) in nuclear cataracts are given as 0.00002% and 0.00003% of the volume respectively. The fact we are missing these structures must be due to this extremely low volume density of these elements.

Advanced cortical cataracts are seen as milky white opacities which extend into the pupillary space and fully obliterate passage of light (Fig. 1; 303, 311, 328). Milky white spots outside the pupillary space (Fig. 1; 316, 321) become apparent in the deep equatorial cortex around the age of 40–50 years and are frequent in the periphery of aging lenses (Vrensen and Willekens, 1990). They are considered as precursors of the spoke-like opacities. Michael et al. (2008) have proposed that these spots are due to mechanical stress at the cortical/nuclear interface at this age when, as shown by Heys et al. (2004), the stiffness of the lens nucleus becomes higher than that of the lens cortex. Scanning and transmission electron microscopy have shown that the spots are relatively small local architectural dispositions of lens fibers as are cortical spoke cataracts due to lens fiber breaks (Brown et al., 1989, 1993; Michael and Bron, 2011). The affected parts of lens fibers are filled with small vesicles and are segregated from unaffected parts of the same fibers (Fig. 3 C and G).

The outcome of the present Raman analysis is that the protein profiles in the fingerprint region of the 5 deep cortical samples, with noticeable opacities, do not deviate from their normal counterparts as shown in Figs. 4 and 5 (deep cortex). Furthermore HC analysis of these samples display no differences in protein profiles of the affected versus the non-affected regions in the sample as exemplified in Fig. 7. Table 2 A shows that the protein mass percentage of the deep cortical samples of lenses with and without cortical opacities is not significantly different. It can be concluded from this evidence that the pathology of the milky white opacities is not accompanied by changes in protein profiles. In a previous Raman study using filipin as a sensitive and specific marker for cholesterol, deep cortical opacities are indeed characterized by a high cholesterol content but not by a higher protein content (Duindam et al., 1998).

The present prevailing concept of nuclear cataract is that oxidative stress and UV lead to changes in crystallins due to a decline in the nucleus of the availability of glutathione (GSH) leading to formation of disulfide bridges (S–S) and ultimately to the aggregation of proteins (Lou, 2003; Michael and Bron, 2011; Truscott, 2000, 2005). The midlife formation of a barrier at the cortical/nuclear interface is suggested to be responsible for this decline in GSH. This concept is supported for chicken, mouse and rat by site specific Raman spectroscopy showing a dramatic drop of

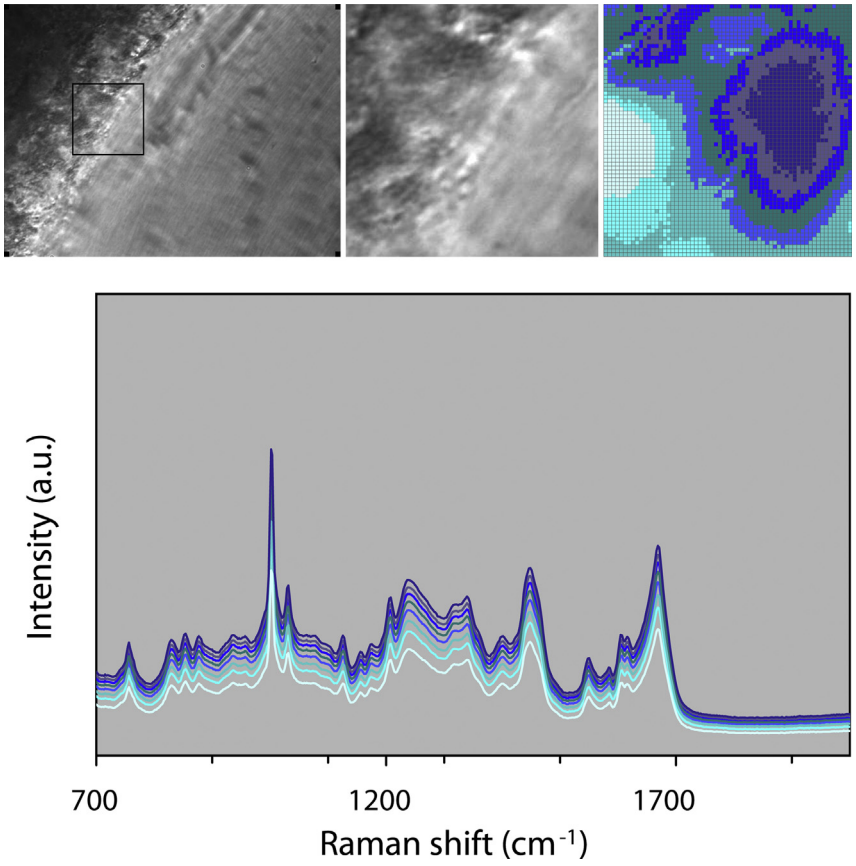

Fig. 7. Hierarchical cluster analyses of a 30 × 30 mm^2 sample of the deep cortex of a lens with an opaque globular region. The spectra in this region do not qualitatively deviate from the normal region. There are some differences in the false color images but as indicated in Fig. 6 they reflect some minor local variations in background and water content.

up to 100% of SH in the nucleus of these species (Askren et al., 1979; East et al., 1978; Kuck et al., 1982; Yu et al., 1985). For humans and guinea pigs this decline is only up to about 25% indicating species differences (Gosselin et al., 2007; Kuck et al., 1982; Yu et al., 1985), also using Raman spectroscopy, showed slightly higher SH concentrations in the nucleus vs. the cortex in guinea pigs. After long term hyperbaric treatment the SH concentration significantly decreases in the nucleus (Gosselin et al., 2007). Inverse observations are found for S–S concentrations: dramatic increases in the lens nucleus of mouse and rat lenses and only slight changes in guinea pig and human lenses. Hyperbaric treatment of guinea pigs also leads to a significant S–S increase in the lens nucleus but not in the cortex. The present Raman study shows that there are no significant differences in SH and S–S content between old human lenses with cortical and nuclear cataracts with differences in coloration and opacities. With respect to S–S we have an unexpected finding: a significant higher value in SC of lenses with cortical cataract. In view of this site specific Raman evidence we can support the view of Yu et al. (1985) that (also in humans) 'opacification of a lens does not necessarily involve the oxidation of sulfhydryl groups or conformational changes in proteins'.

It is well documented that the protein content in the human lens is characterized by a sharp gradient in protein mass percentage (PMP); within 0.5 mm from the capsular surface PMP is rising from 10% in the epithelium and differentiating fibers to a constant level of 40–45% in the cortical and nuclear parts giving a peripheral refractive index of 1.34–1.36 and for the main lens body of up to 1.43 (Augusteyn, 2008; Costello et al., 2012; Fagerholm et al., 1981; Philipson and Fagerholm, 1981). In the present Raman study, using lenses initially fixed in paraformaldehyde and stored in PBS, the PMP is systematically lower than in other studies with a maximum PMP of up to 32–35%. As shown by Augusteyn (2008) preservation in paraformaldehyde leads to a loss in wet weight and is responsible for this lower values. Despite the uncertainty about the absolute values of PMP the present study corroborates the sharp superficial gradient increase in 7 out of the 11 lenses showing a rise in protein mass percentage of 14.6–32.6% between 0.15 and 0.70 mm in the equatorial region. A puzzling observation is the absence of a sharp gradient in 4 out of the 11 lenses (Fig. 9). We searched for a possible correlation factor using age, gender and darkfield characteristics and found that the observed differences are significantly correlated with the absence (lenses 305, 308, 326, 330) or presence (lenses 303, 304, 310, 311, 316, 321, 328) of opacities in the DC (Fig. 9 − and × respectively). As indicated in Table 2 the difference in the superficial cortex is significant at the $p < 0.001$ level with low coefficients of error. This indicates that the difference is unlikely to be ascribed to a few outliers and reflects a more fundamental difference between the 4 lenses with high-protein and the 7 with low-protein content in SC. This could be due to sampling: samples taken a bit deeper in the superficial cortex in these lenses. However, since these 4 lenses all belong to the group with no cortical opacities a sampling problem cannot be excluded but seems unlikely. In a study on human lenses, ranging in age from 9 to 93 years, the surface layer, defined as the distance between the outermost surfaces with lowest PMP to the point PMP has reached its core maximum, was calculated and related to age (Siebinga et al., 1991). In the anterior and posterior poles the surface layer fluctuates around 0.12 mm with no significant change with age. In contrast in the equatorial region the surface layer significantly decreases from 0.6 mm in a 9 year old lens to 0.12 mm in an 85 year old lens. A similar observation is recently described by Augusteyn et al. (2008) using refractive index values measured by

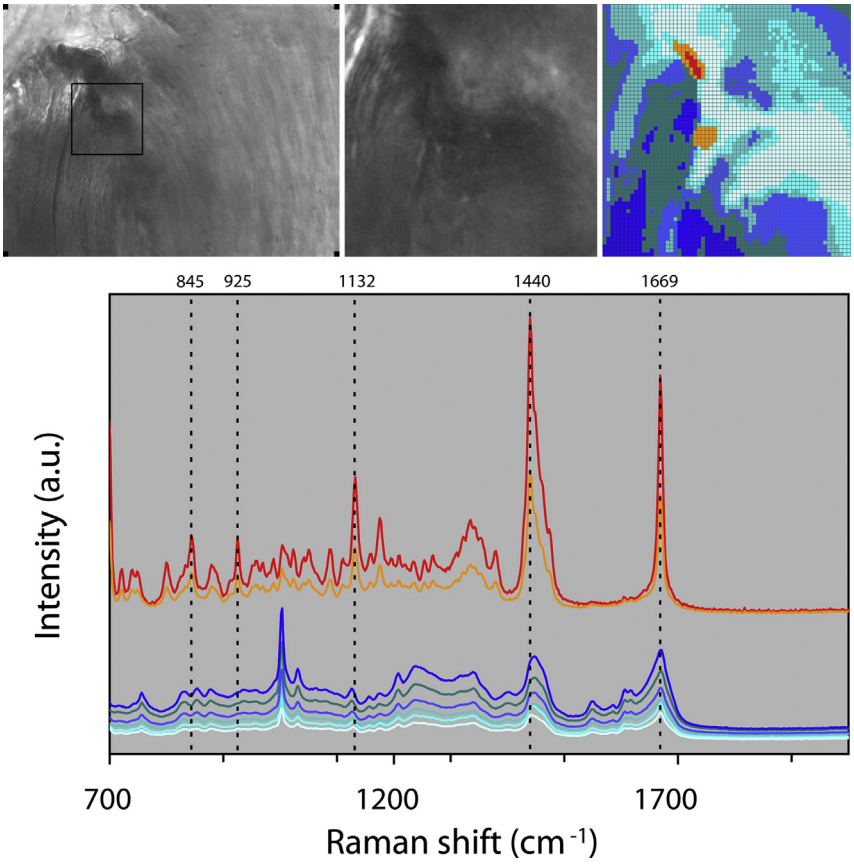

Fig. 8. Hierarchical cluster analyses of a 30 × 30 mm^2 sample of the superficial cortex of a lens close to a suture line (arrows middle image). Two types of spectra are found. The typical blue to white protein profiles as seen in the previous figures and red and orange spectra. The latter have the typical peaks for lipids and cholesterol as given by Bergner et al. (2012). The false color image shows that the phospholipids and cholesterol peaks are locally restricted to two sites in the sample possibly representing a suture line with dense accumulations of membranes.

MRI. It can be discussed that this reflects a decline or arrest in the equatorial mitotic activity and consequently to a decrease in differentiating and maturing cells (Kuwabara, 1975). The higher

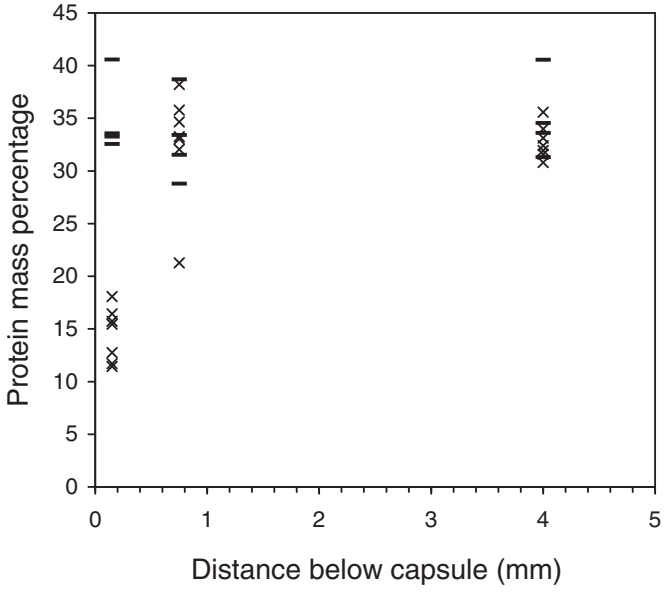

Fig. 9. Protein mass percentage (%) of the 11 lenses analyzed at the superficial cortical, deep cortical and nuclear sites. At the superficial site (0.17 mm) we have four lenses with a PMP of around 35% (−) the other lenses have a PMP of around 15% (×). As described in the discussion and given in Table 2 this difference is significantly correlated with the presence or absence of cortical opacities.

PMP in the lenses with no opacities favors this idea but the question remains why this decrease in surface layer seems more pronounced in the absence of cortical opacities.

As outlined above the present results favor the idea that increased light scatter, as a hallmark of age related nuclear (ARN) cataract, is due to low volume density accumulation of MLB's or protein aggregates. However, it cannot be excluded that changes in the tertiary and quaternary structure of crystallins also contribute. This level of molecular organization can only indirectly be unraveled in situ from studies of the accurate estimation of the α-helix and β-sheet structure (Farnsworth et al., 1997a, 1997b). Fourier transform infrared spectroscopy, circular dichroism and Raman studies have shown that the secondary structure of α-, β- and γ-crystallins mainly consist of α-helices and β-sheets with a preponderance of the latter (Farnsworth et al., 1997a, 1997b; Lamba et al., 1993; Rozyczka and Gutsze, 1991). The present results show a consistent increase with depth of α-helix and β-sheet configurations, except for the SC in cortical cataracts which have higher β-sheet contents (Table 2). These changes may reflect local differences in synthesis of the three types of crystallins (Hockwin et al., 1986; McAvoy, 1978a, 1978b) and formation of high molecular weight crystallins with age (Hockwin et al., 1986; van Kamp and Hoenders, 1973). The age-related increase of tryptophan in the core may reflect a preferential breakdown by endo- and exopeptidases of α-crystallins damaged upon aging. The increase in β-sheet conformation may indicate a post-translational shift in secondary conformation upon aging. These changes in protein conformation are largely completed in a small superficial zone, i.e. in the early life span of the crystallins (Smeets et al., 1993; van Kamp and Hoenders, 1973). More detailed

studies are needed to unravel the role of higher level organization of crystallins on light scatter.

In the absence of consistent changes in protein profiles ubiquitous oxidative changes in crystallins seems not to explain the increased light scatter in age-related nuclear cataracts as advocated by Truscott (Truscott, 2000, 2005). In combination with the observations of (Costello et al., 2010, 2012; van den Berg, 1996; van den Berg and IJspeert, 1995) low density accumulation of protein aggregates or multilamellar bodies is a more plausible explanation for the increased Mie scattering with age and in nuclear cataracts. The absence of significant changes in the protein spectra of cortical opacities and their deviating ultrastructure suggest that these milky white opacities are attributable to the formation vesicle-like elements filled with relatively undisturbed crystallins which cause elastic Tyndall scattering.

Acknowledgement

We are indebted to all donors, to the Banco de Ojos para Tratamientos de la Ceguera, Barcelona and to the Neurological Tissue Bank of the Biobank-Hospital Clinic (NTB-IDIBAPS), Barcelona, for providing the donor eyes.

References

Al-Ghoul, K.J., et al., 1996. Distribution and type of morphological damage in human nuclear age-related cataracts. Exp. Eye Res. 62, 237–251.
Askren, C.C., et al., 1979. Variation of the concentration of sulfhydryl along the visual axis of aging lenses by laser Raman optical dissection technique. Exp. Eye Res. 29, 647–654.
Augusteyn, R.C., 2008. Growth of the lens: in vitro observations. Clin. Exp. Optom. 91, 226–239.
Augusteyn, R.C., et al., 2008. The effect of paraformaldehyde fixation and PBS storage on the water content of the human lens. Mol. Vis. 14, 90–94.
Bassnett, S., 2009. On the mechanism of organelle degradation in the vertebrate lens. Exp. Eye Res. 88, 133–139.
Bassnett, S., et al., 2011. Biological glass: structural determinants of eye lens transparency. Philos. Trans. R. Soc. Lond. B Biol. Sci. 366, 1250–1264.
Bergner, N., et al., 2012. Unsupervised unmixing of Raman microspectroscopic images for morphochemical analysis of non-dried brain tumor specimens. Anal. Bioanal. Chem. 403, 719–725.
Brown, N.P., et al., 1993. Is cortical spoke cataract due to lens fibre breaks? The relationship between fibre folds, fibre breaks, waterclefts and spoke cataract. Eye 7, 672–679.
Brown, N.P., et al., 1989. Lamellar separation in the human lens: the case for fibre folds. A combined in vivo and electron microscopy study. Eye 3, 597–605.
Burd, J., et al., 2012. Simultaneous noninvasive clinical measurement of lens autofluorescence and rayleigh scattering using a fluorescence biomicroscope. J. Diabetes Sci. Technol. 6, 1251–1259.
Costello, M.J., et al., 2012. Electron tomography of fiber cell cytoplasm and dense cores of multilamellar bodies from human age-related nuclear cataracts. Exp. Eye Res. 101, 72–81.
Costello, M.J., et al., 2010. Multilamellar spherical particles as potential sources of excessive light scattering in human age-related nuclear cataracts. Exp. Eye Res. 91, 881–889.
Dahm, R., et al., 2011. Homeostasis in the vertebrate lens: mechanisms of solute exchange. Philos. Trans. R. Soc. Lond. B Biol. Sci. 366, 1265–1277.
Davies, M.J., Truscott, R.J., 2001. Photo-oxidation of proteins and its role in cataractogenesis. J. Photochem. Photobiol. B 63, 114–125.
Delaye, M., Tardieu, A., 1983. Short-range order of crystallin proteins accouts for eye transparancy. Nature 302, 415–417.
Dickson, D.H., Crock, G.W., 1972. Interlocking patterns on primate lens fibers. Invest. Ophthalmol. 11, 809–815.
Dubbelman, M., et al., 2003. Changes in the internal structure of the human crystalline lens with age and accommodation. Vis. Res. 43, 2363–2375.
Duindam, J.J., et al., 1998. Cholesterol, phospholipid, and protein changes in focal opacities in the human eye lens. Invest. Ophthalmol. Vis. Sci. 39, 94–103.
East, E.J., et al., 1978. Raman spectroscopic measurement of total sulfhydryl in intact lens as affected by aging and ultraviolet irradiation. Deuterium exchange as a probe for accessible sulfhydryl in living tissue. J. Biol. Chem. 253, 1436–1441.
Fagerholm, P.P., et al., 1981. Normal human lens – the distribution of protein. Exp. Eye Res. 33, 615–620.
Farnsworth, P.N., et al., 1997a. Effects of temperature and concentration on bovine lens alpha-crystallin secondary structure: a circular dichroism spectroscopic study. Int. J. Biol. Macromol. 20, 283–291.
Farnsworth, P.N., et al., 1997b. Location and exposure of hydrophobic surfaces in relation to an 'open' micellar quaternary structure of alpha-crystallin. Exp. Eye Res. 64, 853–855.
Gosselin, M.E., et al., 2007. Raman spectroscopic evidence for nuclear disulfide in isolated lenses of hyperbaric oxygen-treated guinea pigs. Exp. Eye Res. 84, 493–499.
Heys, K.R., et al., 2004. Massive increase in the stiffness of the human lens nucleus with age: the basis for presbyopia? Mol. Vis. 10, 956–963.
Hockwin, O., et al., 1986. Correlation of Scheimpflug photography of the anterior eye segment with biochemical analysis of the lens. Application of a frozen-sectioning technique to investigate differences in protein distribution of single lens layers. Graefes Arch. Clin. Exp. Ophthalmol. 224, 265–270.
Huizinga, A., et al., 1989. Local variation in absolute water content of human and rabbit eye lenses measured by Raman microspectroscopy. Exp. Eye Res. 48, 487–496.
Kuck, J.F., et al., 1982. Total sulfhydryl by raman spectroscopy in the intact lens of several species: variations in the nucleus and along the optical axis during aging. Exp. Eye Res. 34, 23–37.
Kuszak, J.R., et al., 2004. Fibre cell organization in crystalline lenses. Exp. Eye Res. 78, 673–687.
Kuwabara, T., 1975. The maturation of the lens cell: a morphologic study. Exp. Eye Res. 20, 427–443.
Lamba, O.P., et al., 1993. Estimation of the secondary structure and conformation of bovine lens crystallins by infrared spectroscopy: quantitative analysis and resolution by Fourier self-deconvolution and curve fit. Biochim. Biophys. Acta 1163, 113–123.
Li, L.K., et al., 1985. Membrane cholesterol and phospholipid in consecutive concentric sections of human lenses. J. Lipid Res. 26, 600–609.
Lou, M.F., 2003. Redox regulation in the lens. Prog. Retin. Eye Res. 22, 657–682.
McAvoy, J.W., 1978a. Cell division, cell elongation and distribution of alpha-, beta- and gamma-crystallins in the rat lens. J. Embryol. Exp. Morphol. 44, 149–165.
McAvoy, J.W., 1978b. Cell division, cell elongation and the co-ordination of crystallin gene expression during lens morphogenesis in the rat. J. Embryol. Exp. Morphol. 45, 271–281.
Michael, R., et al., 2008. Morphology of age-related cuneiform cortical cataracts: the case for mechanical stress. Vis. Res. 48, 626–634.
Michael, R., Bron, A.J., 2011. The ageing lens and cataract: a model of normal and pathological ageing. Philos. Trans. R. Soc. Lond. B Biol. Sci. 366, 1278–1292.
Michael, R., et al., 2014. Absence of amyloid-beta in lenses of Alzheimer patients: a confocal Raman microspectroscopic study. Exp. Eye Res. 119, 44–53.
Michael, R., et al., 2003. Changes in the refractive index of lens fibre membranes during maturation–impact on lens transparency. Exp. Eye Res. 77, 93–99.
Philipson, B.T., Fagerholm, P.P., 1981. Human subcapsular cataract – distribution of protein in relation to opacification. Exp. Eye Res. 33, 621–630.
Pully, V.V., et al., 2010. Hybrid Rayleigh, Raman and two-photon excited fluorescence spectral confocal microscopy of living cells. J. Raman Spectrosc. 41, 599–608.
Rozyczka, J., Gutsze, A., 1991. IR spectra of lens crystallins. Lens Eye Toxic. Res. 8, 217–228.
Sasaki, K., et al., 2004. Racial differences of lens transparency properties with aging and prevalence of age-related cataract applying a WHO classification system. Ophthalmic Res. 36, 332–340.
Siddique, M.A., et al., 2010. Phospholipid and protein contents of lens proteolipids in human senile cataract. Eye (Lond) 24, 720–727.
Siebinga, I., et al., 1991. Age-related changes in local water and protein content of human eye lenses measured by Raman microspectroscopy. Exp. Eye Res. 53, 233–239.
Siebinga, I., et al., 1992. Ageing and changes in protein conformation in the human lens: a Raman microspectroscopic study. Exp. Eye Res. 54, 759–767.
Smeets, M.H., et al., 1993. Local variations in protein structure in the human eye lens: a Raman microspectroscopic study. Biochim. Biophys. Acta 1164, 236–242.
Taylor, V.L., et al., 1996. Morphology of the normal human lens. Invest. Ophthalmol. Vis. Sci. 37, 1396–1410.
Truscott, R.J., 2000. Age-related nuclear cataract: a lens transport problem. Ophthalmic Res. 32, 185–194.
Truscott, R.J., 2005. Age-related nuclear cataract-oxidation is the key. Exp. Eye Res. 80, 709–725.
Uzunbajakava, N., et al., 2003. Nonresonant confocal Raman imaging of DNA and protein distribution in apoptotic cells. Biophys. J. 84, 3968–3981.
van den Berg, T.J.T.P., 1996. Depth-dependent forward light scattering by donor lenses. Invest. Ophthalmol. Vis. Sci. 37, 1157–1166.
van den Berg, T.J.T.P., IJspeert, J.K., 1995. Light scattering in donor lenses. Vis. Res. 35, 169–177.
van Kamp, G.J., Hoenders, H.J., 1973. The distribution of the soluble proteins in the calf lens. Exp. Eye Res. 17, 417–426.
van Manen, H.J., et al., 2005. Single-cell Raman and fluorescence microscopy reveal the association of lipid bodies with phagosomes in leukocytes. Proc. Natl. Acad. Sci. U. S. A. 102, 10159–10164.
Vrensen, G., Willekens, B., 1990. Biomicroscopy and scanning electron microscopy of early opacities in the aging human lens. Invest. Ophtalmol. Vis. Sci. 31, 1582–1591.
Vrensen, G.F., 2009. Early cortical lens opacities: a short overview. Acta Ophthalmol. 87, 602–610.
Vrensen, G.F., et al., 2004. Tryptophan deficiency arrests chromatin breakdown in secondary lens fibers of rats. Exp. Eye Res. 78, 661–672.
Yu, N.T., et al., 1985. Disulfide bond formation in the eye lens. Proc. Natl. Acad. Sci. U. S. A. 82, 7965–7968.